Supplementary Information

Ultrafast plasmonic lasing from metal/semiconductor interface

Jian Wang, [a, b] Xiaohao Jia, [c, d] Zhaotong Wang, [e] Weilong Liu, [f] Xiaojun Zhu, [f], Zhitao Huang, [c, d], Haichao Yu, [g] Qingxin Yang, [f] Ye Sun, [e] Zhijie Wang, [c, d] Shengchun Qu, [c, d] Jie Lin, [a, b] Peng Jin, [a, b] Zhanguo Wang [c, d]

[a.] Center of Ultra-precision Optoelectronic Instrument, Harbin Institute of Technology, Harbin 150001, China

[b.] Key Laboratory of Micro-systems and Micro-structures Manufacturing, Ministry of Education, Harbin Institute of Technology, Harbin 150001, China

[c.] Key Laboratory of Semiconductor Materials Science, Beijing Key Laboratory of Low Dimensional Semiconductor Materials and Devices, Institute of Semiconductors, Chinese Academy of Science, Beijing,100083, China.

[d.] Center of Materials Science and Optoelectronics Engineering, University of Chinese Academy of Sciences, Beijing 100049, China

[e.] School of Instrumentation Science and Engineering, Harbin Institute of Technology, Harbin 150080, China

[f.] Department of Physics, Harbin Institute of Technology, Harbin 150080, China

[g] Suzhou Institute of Nano-Tech and Nano-Bionics, Chinese Academy of Sciences, Suzhou 215125, China

Outline

1. Sample preparation

The perovskite nanowires were grown using electrochemical assisted solution method reported in our previous report[1]. At first, the PbO_2 thin film was deposited on ITO substrate by the electrochemical method and then the synthesized PbO_2 film was put in $CH_3NH_3Br_3$ isopropyl solution. After 4 hours growth, the single crystalline $CH_3NH_3PbBr_3$ nanowires were synthesized. All of the nanowires under optical characterizations had length in the range from 4μm to 15μm and their aspect ratio is about 1:1.3. The single crystal Ag plates were synthesized using a platinum nanoparticle catalyzed and ammonium hydroxide-controlled polyol reduction method[2, 3]. Ag plates were purged using acetone, alcohol and deionized water for three cycles

after the reaction was completed. Then we dispersed Ag plates in alcohol on a silicon substrate in the glovebox. After the alcohol was evaporated, we transferred the $CH_3NH_3PbBr_3$ nanowires from as-grown substrate to Ag plates by a dry process to establish SPP lasers.

SEM images were collected on a Zeiss Sigma field emission SEM operated at 5.0kV. The XRD patterns were acquired on a Panalytical X' Pert Pro diffractometer. The AFM images were acquired on a Bruker Dimension ICON AFM using tapping mode. The scan area is $5\times5\mu m^2$ and root-mean-squared (RMS) roughness values were extracted by Nanoscope Analysis software.

2. Optical characterizations

The 400nm excitation light was generated from the second harmonic of the fundamental output (800nm central wavelength, nominally 130fs pulse duration and 1kHz repetition rate) from a regenerative amplifier (Spectra-Physics Spitfire amplifier seeded by Tsunami oscillator). The excitation light was focused onto the nanowire by a 40×, NA = 0.65 objective and the circular beam could cover a single nanowire completely. The emission from each nanowire was collected by the same objective and focused into a spectrograph (Princeton Instrument, Acton SP2300i) with a $300mm^{-1}$ grating and a liquid-N2-cooled CCD (PyLoN 400B). A linear polarizer was placed before the spectrograph slit to analyze polarization of emitted light. For the double-pump experiments, the 400nm pump light was split to two beams by a 5:5 beam splitter. One of them was sent through a delay line with a minimum scanning step size equivalent to 13.3fs. Both beams were joined using collinear configuration through a beam

splitter and focused through the same objective as mentioned above. The emitted light of double pump experiments was also collected using Acton SP2300i. The power ratio of the two pump pulses was fixed at 5:1.

3. Transverse mode profiles and mode characteristics of the SPP laser

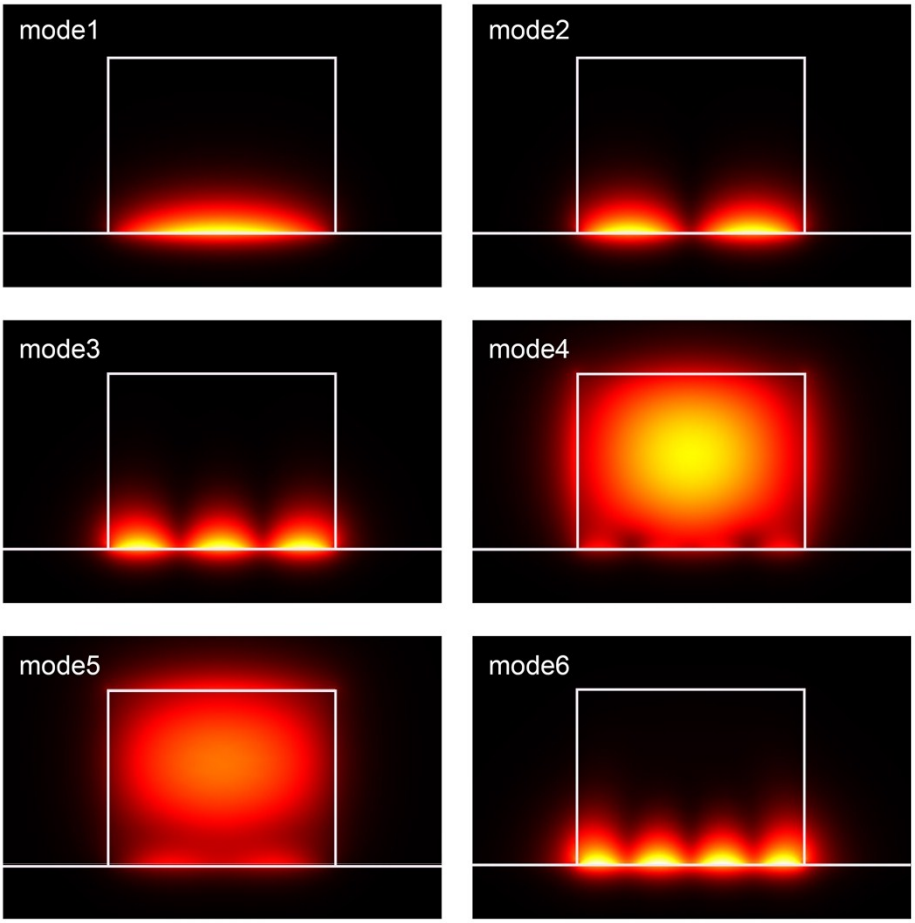

Fig. S1 Transverse mode patterns of a nanowire placed on an Ag film directly.

We simulated the mode profiles of a single $CH_3NH_3PbBr_3$ nanowire on an Ag film with the incident wavelength of 540nm. The refractive indexes of $CH_3NH_3PbBr_3$ perovskites and silver were taken from previous reports[4, 5]. The height of the nanowire was 150nm and the aspect

ratio was set to be 1:1.3. The six sustainable transverse modes of the plasmonic lasers are shown in Fig. S1. Besides of the fundamental mode (shown in Fig. 1c) marked as mode1, other high order modes such as mode2, mode3 and mode6 are highly localized at the interface of the Ag film and the nanowire indicating very strong confinement effect and light-matter interaction. We name the four modes as MODE1. The other two modes (mode4 and mode5), which demonstrate distributions of electric fields not only at the interface but also in the nanowire, seem to be the combination of plasmonic modes and guided modes in a freestanding nanowire. We name the two modes as MODE2. Then the characteristics of these modes against the height of the nanowire were calculated and the results are shown in Fig. S2

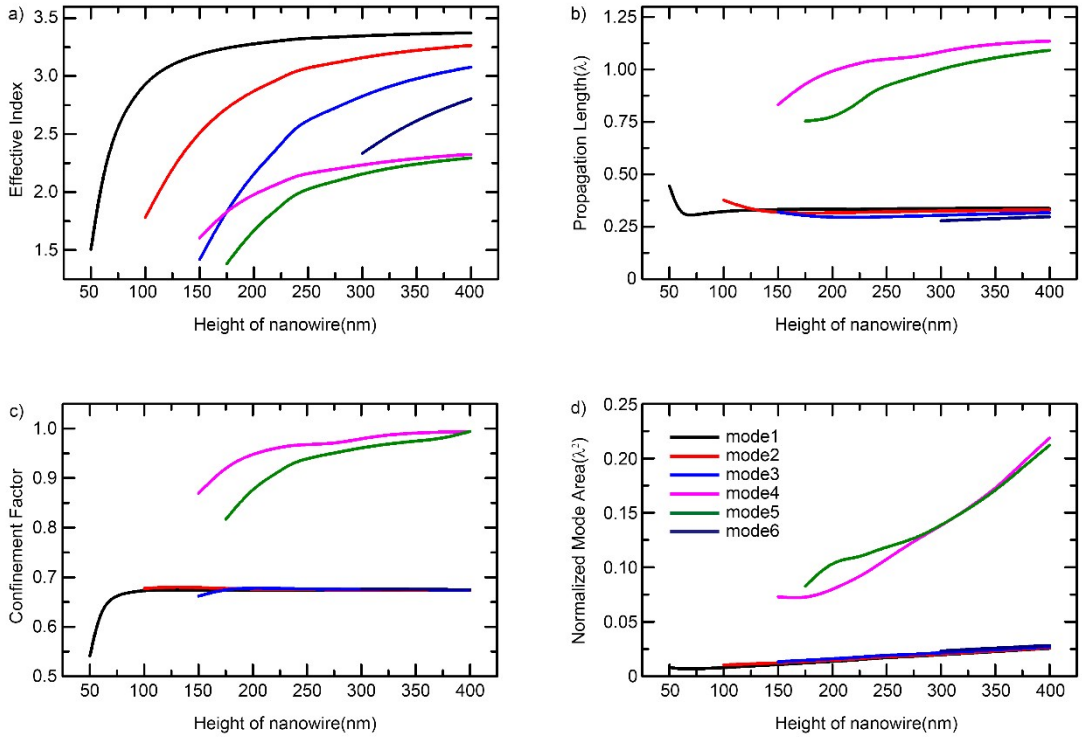

Fig. S2 Mode characteristics versus the height of nanowire with the incident wavelength at 540nm. a) The effective index. b) The propagation length. c) The confinement factor and d) The mode area.

Mode characteristics including the effective index, the propagation length, the confinement factor and the normalized mode area are shown in Fig. S2. The mode area[6] and confinement factor[7] are the same as the ones defined in ref. 1 and ref. 2. It's clear that the mode characteristics of MODE1 are different from those of MODE2. The MODE1 experiences a bigger effective index, shorter propagation length, and smaller confinement factor and mode area. In this case, the smallest mode area is 38 times smaller than a diffraction limited area in vacuum ($\lambda^2/4$).

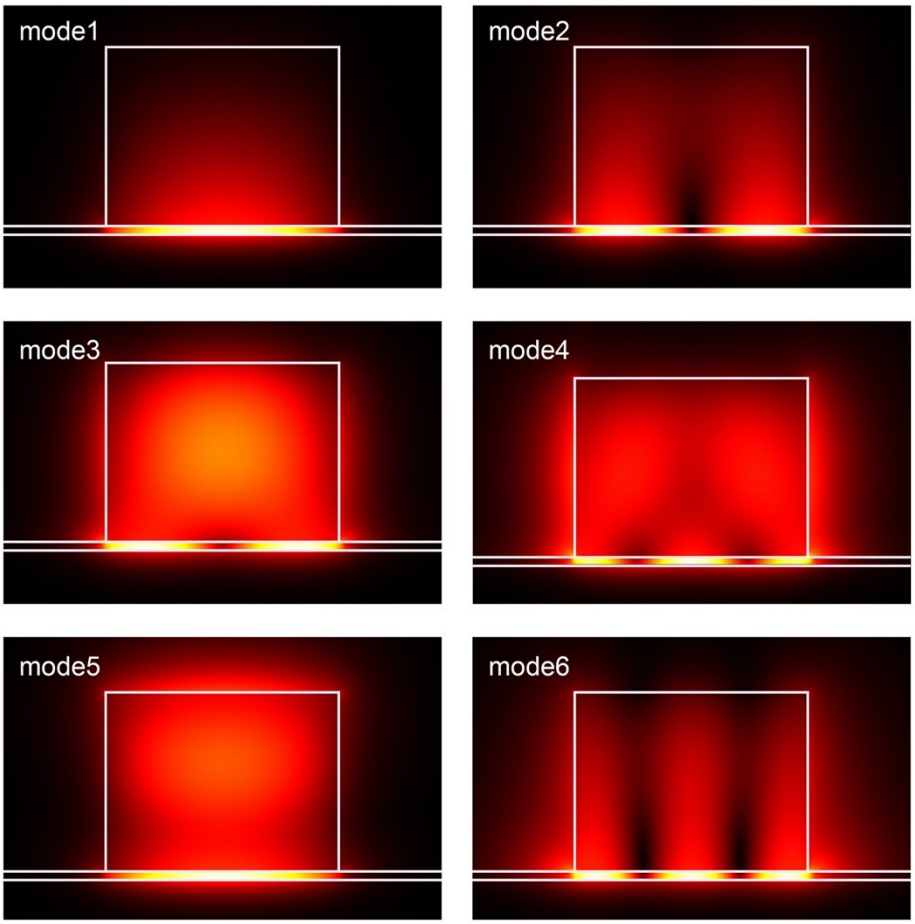

Fig. S3 Transverse mode profiles of hybrid plasmonic laser

The transverse mode profiles of hybrid plasmonic lasers which consist of a $CH_3NH_3PbBr_3$ nanowire on silver film separated by a nanoscale MgF_2 layer are shown in Fig. S3. The height of the nanowire is 250nm and the thickness of the MgF_2 layer is 10nm. The mode characteristics of the fundamental mode of nonhybridized and hybrid plasmonic lasers with the MgF_2 layer of different heights against height of the nanowire are shown in Fig. S4 for comparison. The height of the MgF_2 layer is set to be 5nm, 10nm and 20nm respectively.

Fig. S4 indicates that nonhybridized plasmonic lasers are able to realize stronger confinement effect than hybrid counterparts because nonhybridized plasmonic mode has larger wave vector and greater confinement factor for the same mode area, which is consistent with Fig. 1b in main text.

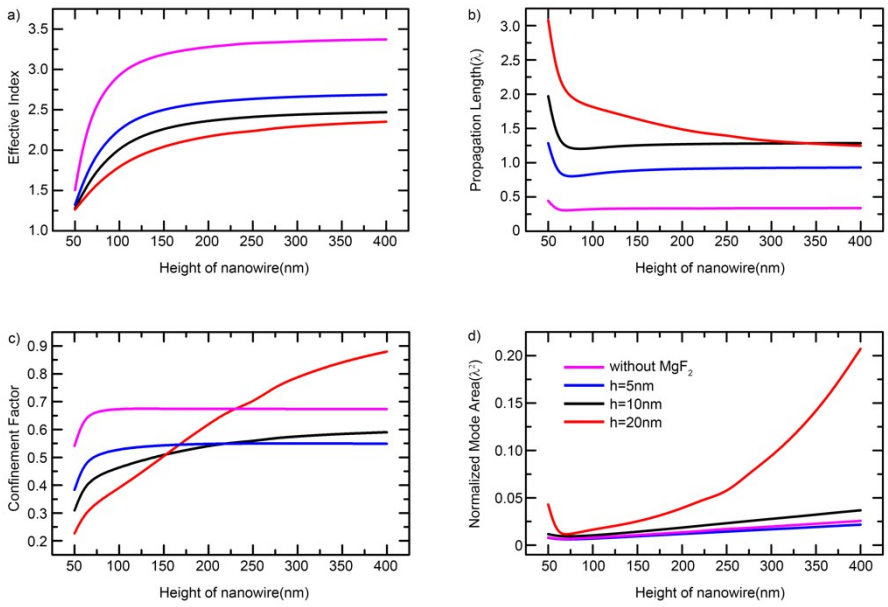

Fig. S4 Mode characteristics of nonhybridized and hybrid plasmonic lasers. a) The effective index. b) The propagation length. c) The confinement factor and d) The mode area.

The dominant electric field components are perpendicular to the metal surface and parallel to the nanowire axis, as shown in Fig. S5a and S5b, indicating the fundamental nonhybridized plasmonic mode[8, 9].

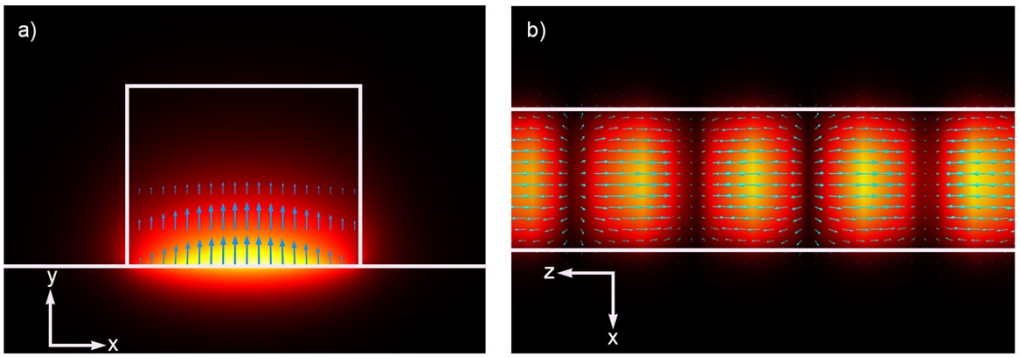

Fig. S5 Simulated electric field distribution of fundamental SPP mode. a) and b) are distributions of |E| field of plasmonic modes in the x/y and x/z planes. The arrows indicate the direction of |E| field. The orientation of polarization of electric filed is perpendicular to the metal surface and parallel to the nanowire axis. The axes labels are determined according to the coordinate of Fig 1a in main text.

4. Additional information of materials characterization

SEM images of Ag plates, XRD of as-grown $CH_3NH_3PbBr_3$ nanowires and SEM images of SPP lasers are shown in Fig. S6 and Fig. S7.

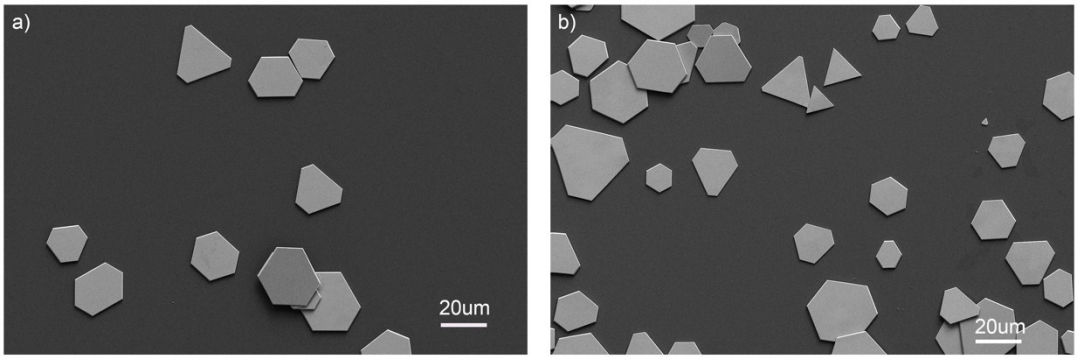

Fig. S6 SEM images of Ag plates on the silicon substrate

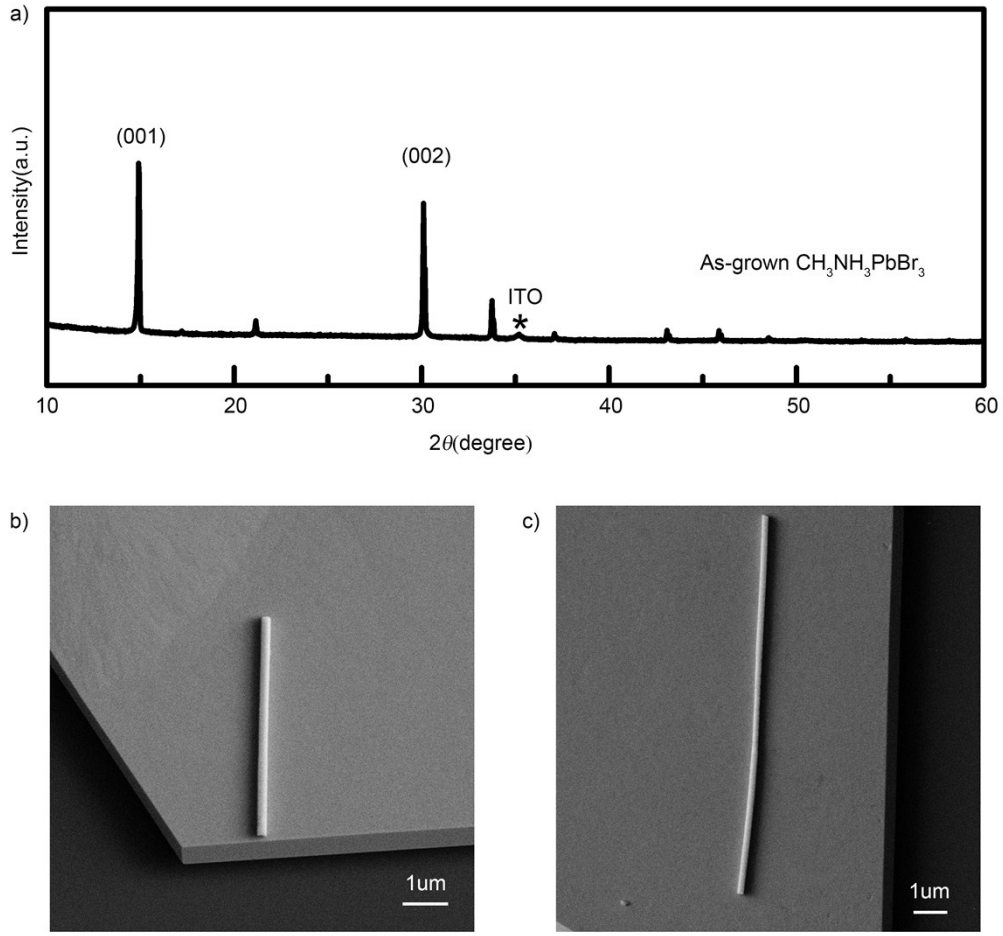

Fig. S7 XRD of perovskite nanowires and SEM images of SPP lasers. a) XRD pattern of as-grown $CH_3NH_3PbBr_3$ nanowires. The sharp (001) peak and (002) peak confirm the cubic phase of the perovskite material without any impurity phase. b) and c) show the SEM images of plasmonic nanowire laser devices consist of a single $CH_3NH_3PbBr_3$ nanowire placed on Ag

plate directly.

5. Dependence of mode spacing on nanowire length

The mode spacing has an approximately linear relationship with inverse nanowire length of all measured plasmonic lasers as shown in Fig. S8 which indicates the Fabry-Pérot like cavity behavior. From this figure, the average group index was estimated to be around 9.1.

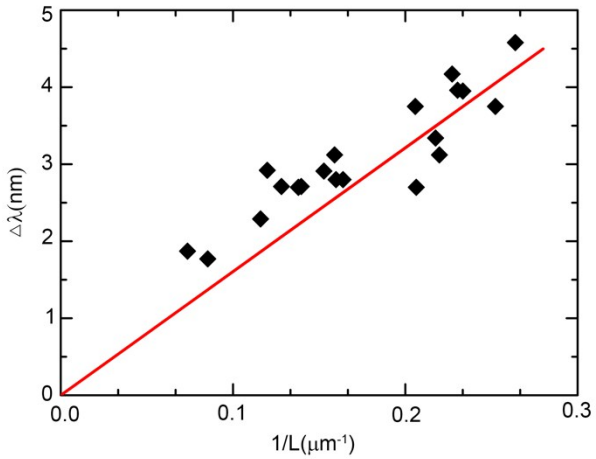

Fig. S8 Mode spacing versus inverse nanowire length

6. Additional information of optical characterizations

We measured the double pump response of the hybrid plasmonic laser at two times threshold. The temporal response is shown in Fig. S9. From the exponential fitting, the radiative decay rate is about 19.0ps, which is slower than counterpart of the nonhybridized plasmonic lasers.

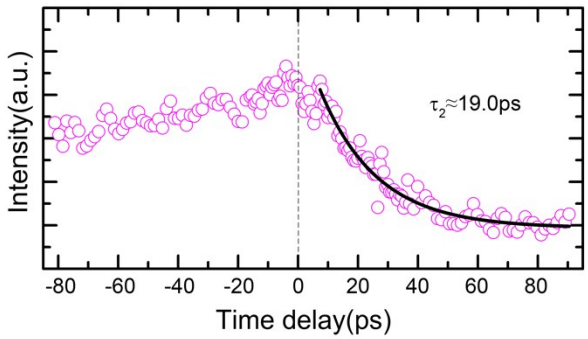

Fig. S9 Temporal response of the hybrid plasmonic laser

Another typical result of nonhybridized SPP lasers including static emission spectra and the dynamic temporal response are shown in Fig. S10. Fig. S10a shows spectra evolution of the SPP laser from spontaneous emission via amplified spontaneous emission to full laser oscillation along with increasing pump intensity. The integrated emission intensity and FWHM of laser peaks against pump intensity are presented in Fig. S10c, showing the lasing threshold at around 0.86mJ/cm^2. The electric field with polarization parallel to the nanowire axis (red curve) and with polarization perpendicular to the nanowire axis (black curve) excited at 1.9P_{th} are shown in Fig. S10b, indicating realization of the plasmonic laser. The double-pump response of the same SPP laser at 1P_{th} and 2P_{th} are shown in Fig. S10d. This figure shows the same phenomena including ultrafast decay rate and pump density dependent peak response time as Fig. 4 in main text. Besides, we measured spectral-temporal response of the same SPP laser as shown in Fig. S11, which demonstrated varying peak response time with increasing pump intensities.

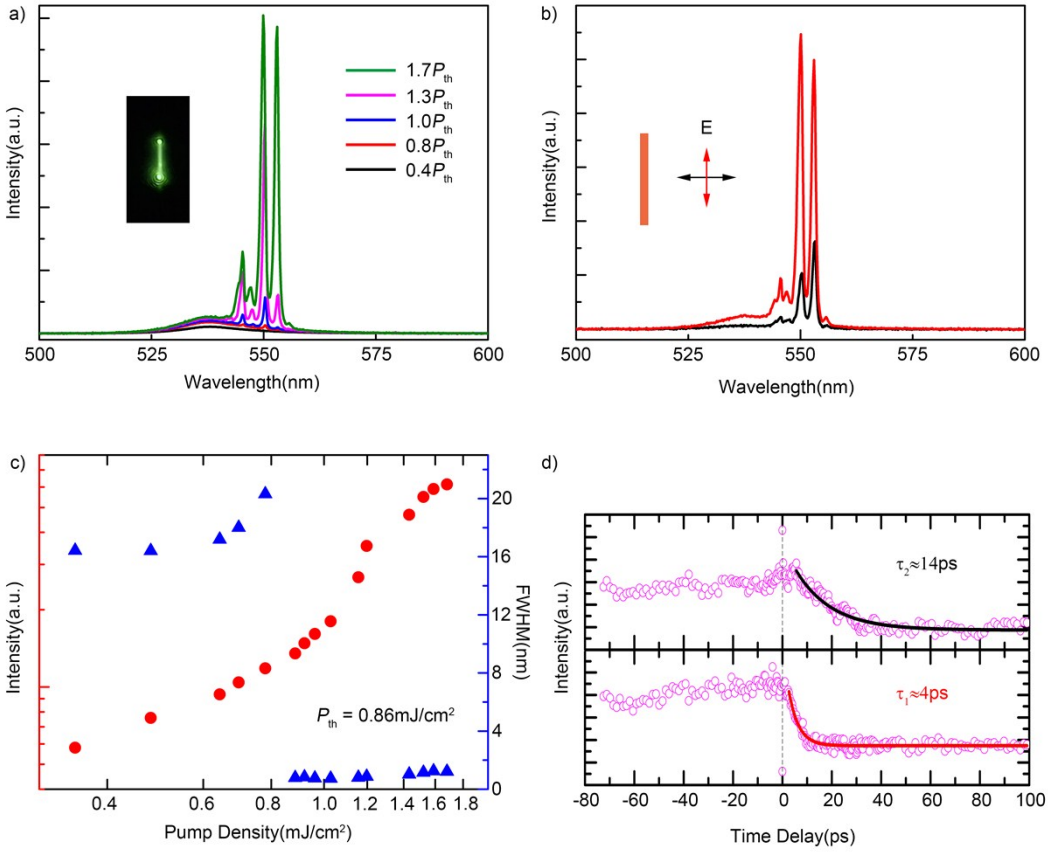

Fig. S10 Static lasing characteristics and the dynamic temporal response of SPP laser. a) Emission spectra of SPP laser against different pump density. The inset shows the optical image of the laser above the threshold value. b) Polarization-sensitive lasing spectra at room temperature, with red curve parallel to the nanowire axis and black curve perpendicular to the nanowire axis. c) Integrated spectra intensity and FWHM versus the different pump density showing the threshold at 0.86 mJ/cm^2. d)The temporal response of SPP laser at two different pump densities ($1P_{th}$ and $2P_{th}$).

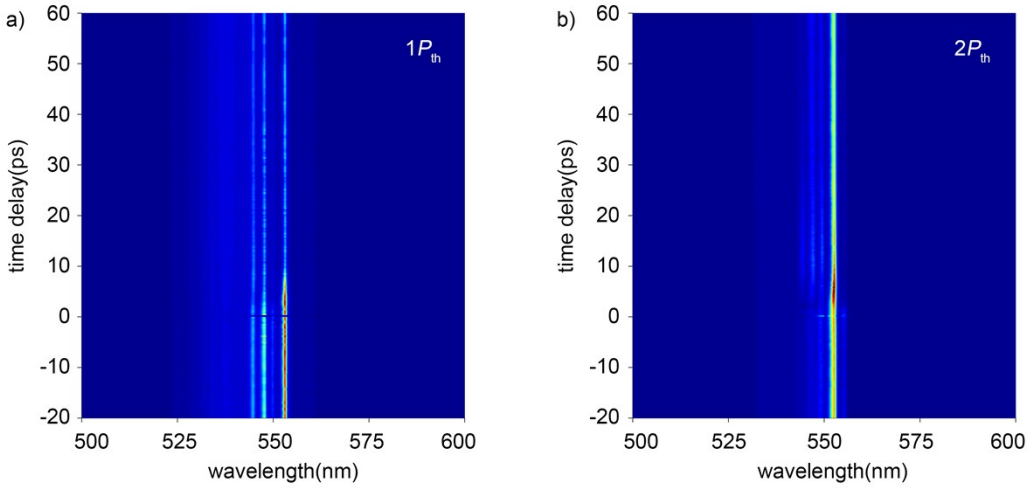

Fig. S11 The spectral-temporal lasing response at different pump intensity of the same device in Fig. S8. a) response map at $1P_{th}$. b) response map at $2P_{th}$

7. Rate equations

We use a simplified rate equation[7, 10, 11] to describe the dynamic evolution of the SPP laser dependent on pump density.

$$\frac{dn}{dt} = \sigma p - An - \Gamma As(n - n_0) \quad (1)$$

$$\frac{ds}{dt} = \beta An + \Gamma As(n - n_0) - \gamma s \quad (2)$$

Where n is the carrier density, s is the photon density. Here, A is the average spontaneous emission rate and n_0 is carrier concentration when the gain medium is transparent. Γ is the gain overlap factor, and γ is the sum of the propagation and cavity loss rate. β is the spontaneous emission factor and σ is the pump photon to laser photo conversion efficiency. We solved these equations for an incident pump laser pulse, $p(t) = p_0 \exp(-(t - t_0)^2 / \Delta t^2)$.

8. Thresholds with nanowire dimensions

Fig. S12 shows the threshold performance against the height and width of the nanowire.

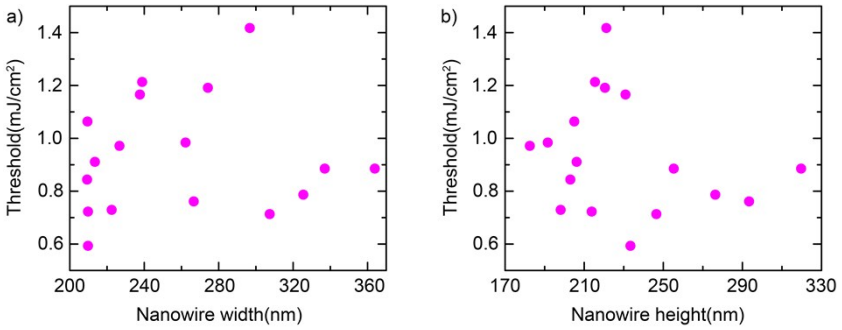

Figure S12 Threshold against the height and width of the nanowire. a) threshold versus nanowire width; b) threshold versus nanowire height

References

(1) Ren, K.; Wang, J.; Chen, S.; Yang, Q.; Tian, J.; Yu, H.; Sun, M.; Zhu, X.; Yue, S.; Sun, Y.; Liu, K.; Azam, M.; Wang, Z.; Jin, P.; Qu, S.; Wang, Z. Realization of Perovskite-Nanowire-Based Plasmonic Lasers Capable of Mode Modulation, *Laser Photonics Rev.* **2019,** 13, (7), 1800306.

(2) Jin, L. H. Z. K. D.; Chung Hun, S.; LiShao, Z. J. Y. K. N.; Xing, H. L. R. Mechanism for the Formation of Flake Silver Powder Synthesized by Chemical Reduction in Ethylene Glycol, *Acta Phys.-Chim. Sin.* **2003**, (2), 11.

(3) Wang, C.-Y.; Chen, H.-Y.; Sun, L.; Chen, W.-L.; Chang, Y.-M.; Ahn, H.; Li, X.; Gwo, S. Giant colloidal silver crystals for low-loss linear and nonlinear plasmonics, *Nat. Commun.* **2015,** 6, 7734.

(4) Yang, Y.; Yan, Y.; Yang, M.; Choi, S.; Zhu, K.; Luther, J. M.; Beard, M. C. Low surface recombination velocity in solution-grown CH 3 NH 3 PbBr 3 perovskite single crystal, *Nat. Commun.* **2015,** 6, 7961.

(5) Johnson, P. B.; Christy, R.-W. Optical constants of the noble metals, *Phys. Rev. B* **1972,** 6, (12), 4370.

(6) Oulton, R. F.; Sorger, V. J.; Genov, D.; Pile, D.; Zhang, X. A hybrid plasmonic waveguide for subwavelength confinement and long-range propagation, *Nat. Photonics* **2008,** 2, (8), 496.

(7) Oulton, R. F.; Sorger, V. J.; Zentgraf, T.; Ma, R. M.; Gladden, C.; Dai, L.; Bartal, G.; Zhang, X. Plasmon lasers at deep subwavelength scale, *Nature* **2009,** 461, (7264), 629-32.

(8) Chou, Y. H.; Wu, Y. M.; Hong, K. B.; Chou, B. T.; Shih, J. H.; Chung, Y. C.; Chen, P. Y.; Lin, T. R.; Lin, C. C.; Lin, S. D.; Lu, T. C. High-Operation-Temperature Plasmonic Nanolasers on Single-Crystalline Aluminum, *Nano Lett.* **2016,** 16, (5), 3179-86.

(9) Ho, J.; Tatebayashi, J.; Sergent, S.; Fong, C. F.; Iwamoto, S.; Arakawa, Y. Low-Threshold near-Infrared GaAs–AlGaAs Core–Shell Nanowire Plasmon Laser, *ACS Photonics* **2014,** 2, (1), 165-171.

(10) Yokoyama, H.; Brorson, S. D. Rate equation analysis of microcavity lasers, *J. Appl. Phys.* **1989,** 66, (10), 4801-4805.

(11) Yu, H.; Ren, K.; Wu, Q.; Wang, J.; Lin, J.; Wang, Z.; Xu, J.; Oulton, R. F.; Qu, S.; Jin, P. Organic–inorganic perovskite plasmonic nanowire lasers with a low threshold and a good thermal stability, *Nanoscale* **2016,** 8, (47), 19536-19540.